J Appl Electrochem (2007) 37:949–959
DOI 10.1007/s10800-007-9335-z

ORIGINAL PAPER

Electrochemical investigations on composite iron electrodes

N. Comisso · G. Mengoli

Received: 15 November 2006 / Revised: 25 April 2007 / Accepted: 27 April 2007 / Published online: 24 May 2007
© Springer Science+Business Media B.V. 2007

Abstract In spite of the many studies performed since the beginning of the last century, the Fe electrode, used as negative of both Ni/Fe and Fe/Air batteries, still poses several problems. For instance, according to the current literature, the following points are still not clear: (i) whether and how the depth of discharge affects electrode performance; (ii) what pathway the discharge follows, generally assumed as it is to involve consecutive $Fe \rightarrow Fe^{II}$ and $Fe^{II} \rightarrow Fe^{III}$ oxidation; (iii) why, at room temperature, only a minor fraction of the large theoretical capacity can be exploited. The present paper shows that deep discharges do increase Fe electrode performance, since they induce a transitory inhibition of hydrogen evolution. Likewise, Fe/Metal oxide composite electrodes have shown that the formation of Fe^{III} in discharge can take place directly from Fe, when the discharging rate applied is no longer compatible with the increase in electrode resistance due to oxidation products. Fe/Intermetallic compound composite electrodes have been studied as possible routes for increasing the efficiency of Fe capacity: useful indications have been gained as regards the compatibility of Fe with an IMC for charge storage.

Keywords Electrochemistry · Iron · Oxides · Intermetallic · Hydrogen

1 Introduction

For most applications, alkaline Ni/Cd and, recently, Ni/Metal hydrides have superseded the old Ni/Fe battery [1–3], whose major drawback is the thermodynamic instability of iron in aqueous electrolytes. This instability, due to the close proximity of the Fe electrode potential to that of hydrogen, has practical consequences of:

- low charge/discharge efficiency for the hydrogen evolution reaction (h.e.r.), overlapping the main process of Fe^{II} reduction;
- high self-discharge rate of Fe corroded by the aqueous environment.

Nevertheless, the Ni/Fe battery is still attractive, as it combines reasonable energy density with outstanding robustness, high environmental safety and unlimited material (Fe) availability. For these reasons it is also at present the subject of research and development in countries where the above properties are considered of prevailing importance.

In addition, when coupled to the oxygen electrode, the Fe electrode constitutes a promising system among metal/air batteries [4–7], since Fe has better electrochemical reversibility than Zn or Al, and Fe/Air approaches the energy density requirements of vehicular traction, where self-discharge and charging efficiency pose fewer problems than in stationary applications.

The development in the Fe/Air battery of the positive (Air) electrode can now exploit progress in alkaline fuel cell technology but, in spite of the considerable work from the beginning of the last century to the 1980s [1–3] in the West and nowadays also in other countries [8–13], the negative Fe electrode still represents a challenge, not only for applications but also for fundamental research.

Success has been achieved in the manufacture of Fe electrodes with improved performance, but technological progress has often not been accomplished with deeper knowledge of the system. For instance, the beneficial effect

N. Comisso (✉) · G. Mengoli
CNR IENI, Corso Stati Uniti 4, Padova 35127, Italy
e-mail: nicola.comisso@ieni.cnr.it

to the Ni/Fe battery of the presence of Li^+ ion in the electrolyte has been known since the times of Thomas Edison [14], but the reason for such effects has only recently been explained [15].

The present work re-examines some aspects of the Fe electrode which appear to be either contradictory or puzzling. For instance, it is still not clear whether and how the depth of discharge affects electrode performance: although the Fe/Ni oxide battery is claimed to tolerate overcharging and overdischarging easily [3], the Fe electrode is elsewhere [16] reported to undergo irreversible passivation when discharged above –0.60 V (versus Hg/HgO). The discharge limit and correct charging/discharging procedures are important, since they affect the efficiency and life of the electrode.

A second point examined here is the complete discharging pathway of Fe, which is generally assumed to involve two main oxidation steps, i.e., $Fe \rightarrow Fe^{II}$ (the useful semi-cell reaction) and $Fe^{II} \rightarrow Fe^{III}$. These steps should be in ratios of 3:1 (when Fe_3O_4 is formed as final product) or 2:1 (with FeOOH or Fe_2O_3 as final products), but this point does not appear to have been studied in sufficient depth.

Lastly, this work investigated the fact that, at room temperature (25 °C), only a minor fraction of the large theoretical capacity (960 mA h g^{-1}) of the $Fe \rightarrow Fe^{II}$ reaction is actually available: the fraction generally ranges from $\leq 30\%$ for pressed powder electrodes to $\leq 50\%$ for advanced sintered electrodes. If extensive exploitation of nominal capacity is not required in the Fe/Ni oxide battery, where the capacity of the positive (NiO) electrode is far lower (294 mA h g^{-1}), the same is not true for the practical Fe/Air system for traction, which requires the energy density to be as high as possible.

2 Experimental

2.1 Materials

The study was carried out on Fe powder (sizes ≤ 100 μm) especially designed for battery use by SAFT-NIFE (Sweden). As shown by the X-ray diffraction pattern of Fig. 1, the material mainly consists of pure metal iron with minor amounts of Fe oxides. X-ray data were obtained on a Philips PV 3710 instrument (CuKα radiation, 40 KV, 30 mA). Traces of sulphur were detected in the sample by EDAX/EDS analysis.

Self-standing Fe powder electrodes were prepared by inserting a weighed amount of powder into a weighed strip of Ni foam (from Sorapex), followed by pressing in a hydraulic press at 200–300 bar and fixing by immersion in a dilute solution of epoxy resin. The Fe content of the strip was 70–80% of the total weight. Square-cut from the strip according to the chosen dimensions and pressure-bonded to a Ni wire, it then constituted the self-sustaining Fe electrode sample suitable for electrochemical study.

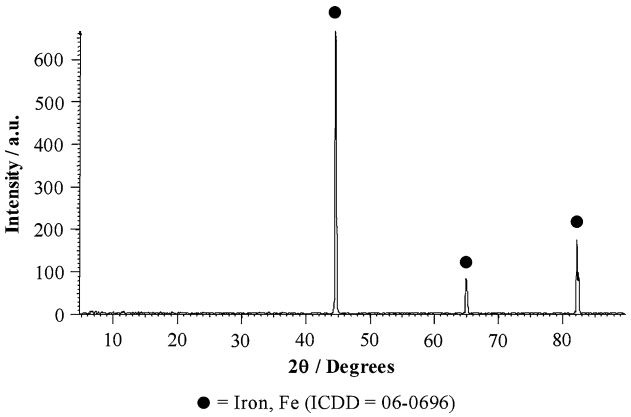

Fig. 1 X-ray diffractogram of the Fe (SAFT-NIFE) sample utilized in the work

Fe powder was also studied, not only by itself, but also in composites prepared with powder of: TiO_2 (rutile) from Kronos 1002; Al_2O_3 from Buehler (<1 μm); ZrO_2 from Sigma-Aldrich (<5 μm, 99%); ZnO from Merck (99%); $LaNi_5$ from Johnson Matthey (–100 mesh, 99.5%) and NiTi from Goodfellow (500 μm).

The powder mixtures were generally made by milling the samples for 1 hour at 150 rpm in an Ar atmosphere in a planetary mill (Pulverisette 7, Fritsch), in 25-mL tungsten carbide bowls equipped with 7 tungsten carbide balls (ϕ = 12 mm). TiNi was previous milled alone owing to its hardness. All the milling operations were performed at room temperature.

2.2 Electrolyte

The chemicals used for preparing solutions were KOH and LiOH, reagent grade, from Fluka, and H_2O, of Millipore grade. Typical electrolyte composition was KOH 4.0 M + LiOH 2.0 M: although other KOH/LiOH ratios are also used in both Ni/Fe Fe/Air batteries [1], the 4 M/2 M mixture was adopted here, since it had already been tested successfully for reducing various Fe oxides [15]. For instance, Fig. 2 compares results obtained at 25 °C with the same Fe_3O_4 pressed powder electrode submitted to galvanostatic reduction, either in KOH 6.0 M alone or in KOH 4.0 M + LiOH 2.0 M. In the former case (curves a, a′), prolonged reduction followed by galvanostatic anodisation did not reveal any significant oxidation process, since no metallic iron was actually achieved after reduction. In the latter case (curves b, b′), the oxidation curve, after shorter reduction, showed that a good amount of

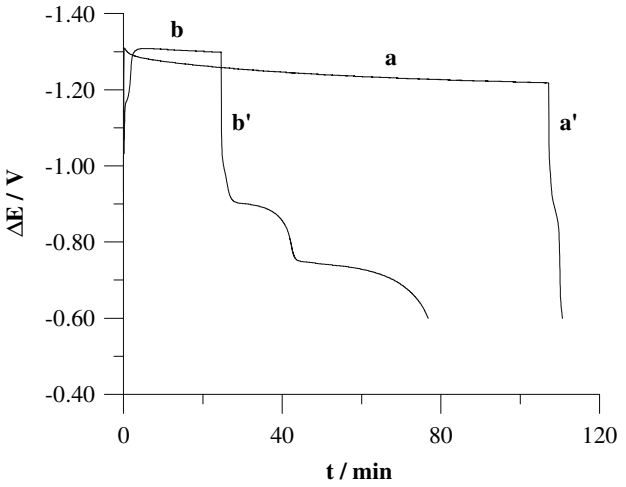

Fig. 2 Charging/discharging patterns at 25 °C of a magnetite (Fe_3O_4 content = 0.135 g) pressed powder electrode in: a/a′ (–200/+20 mA) in KOH 6.0 M; b/b′ (–200/+10 mA) in 4.0 M KOH + 2.0 M LiOH

magnetite had been converted into Fe by the Li^+ ion, probably through an intercalation-decomposition process.

2.3 Apparatus and procedure

The Fe or Fe composite sample electrode was submitted to galvanostatic charging/discharging (reduction/oxidation) cycles in an uncompartmented cylindrical cell made of polyethylene with ≈150 ml useful capacity. The sample, placed in the middle of the cylinder, constituted the working electrode; the counter electrode was a Ni coil (ϕ = 0.1 cm, length = 50 cm) rolled around the former. The reference electrode, placed near the working electrode, was a Hg|HgO|KOH (0.1 M) electrode manufactured by AMEL (Milan). Working and reference electrodes were interfaced with a PC, to monitor working electrode potential at any time during electrolysis. The cell was sealed at the top by a Teflon lid, which supported electrodes, electrical connections and an inlet/outlet tube system, allowing both exit of the gas produced by H_2O discharge or, when required, inflow/outflow of N_2 (by Air Liquide, 99.999% purity) across the electrolyte. The body of the cell was kept at 25 °C by a Haake F3 thermostat in a silicon oil bath.

Steady-state potentiodynamic curves were achieved, always at 25 °C, in a Pyrex cell with the working electrode compartment maintained under a continuous flow of N_2, separated from that of the counter electrode (a Ni plate) by a porous glass frit. The working electrode compartment was connected to the reference electrode (Hg|HgO) through a Luggin capillary. Potentiodynamic curves were achieved by points, by recording the current attained after 3 min of potentiostatic electrolysis at each potential. On this cell only the cathode compartment was double-jacketed in order to allow thermostatic temperature control.

Electrochemical instrumentation consisted of Amel or EG&G/Princeton Applied Research model 273A apparatus, both interfaced with a PC.

3 Results

3.1 Pure Fe powder electrode

3.1.1 Activation

The evolution of the charge capacity of a pure Fe powder electrode with the number of charging/discharging cycles was studied in the conditions described below:

- sample characteristics: dimensions = 0.60 × 2.00 cm^2, net Fe content = 0.207 g, with theoretical capacity = 199.7 mA h, assuming that all powder was metallic iron;
- two charging programs, both in excess of what was required by nominal capacity of sample electrode, i.e., fast charging with –200 mA (0.966 A g^{-1}) applied for 1 h, and slow charging with –40 mA (–0.193 A g^{-1}), applied overnight (≈15 h);
- discharge followed charge immediately, and was performed in the range of 40 mA rate;
- charge capacity considered was integrated to –0.800 V (versus Hg|HgO), i.e., to inflection of Fe → Fe^{II} potential plateau;
- the parameter which varied from time to time during the experiment was the anodic limit of discharge (see Fig. 4), increased in the succession –0.60 V, –0.40 V, –0.20 V, and then decreased to –0.75 V.

These results are shown in Fig. 3, which gives charge capacity (as a percentage of the theoretical value) according to the progressive number of cycles: full dots represent charge after fast electrode charging and empty dots after slow charging.

Therefore, with –0.60 V as the anodic limit after the initial 10–15 cycles, the rate of activation slows still further, as the reversible charge storage approaches 15–16% of theoretical capacity. With discharge extended to –0.40 V, storage increases to between 25–30%, the second figure being obtained after long slow charging. With –0.20 V as the most anodic limit, storage eventually settles at between 30% and 40%, the highest value again being achieved after charging the electrode slowly for ≈15 h.

When the anodic potential was reduced back to –0.75 V, so as to restrict charge extraction to the plateau of the Fe → Fe^{II} process, after an initial drop, storage then showed a much smoother decline, which was offset by a long reduction time: in this way, charge capacity could be maintained at around 30% of the theoretical value. Clearly,

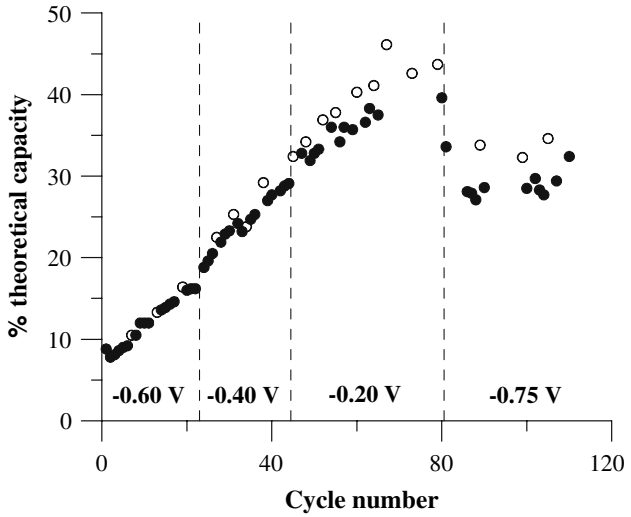

Fig. 3 Evolution of Fe sample charge capacity (as percent of the theoretical prevision) with number of charging/discharging cycles for different anodic limits of the discharges. Full dots represent capacity data obtained by discharge following fast rate charging (see the text); empty dots are data obtained after prolonged slow rate charging

full recovery of maximum storage was always obtained by again increasing the anodic limit of discharge.

It therefore appears that a high anodic limit has beneficial effects on both the rate of Fe activation to maximum charge storage and on the maintenance of this capacity. This is also shown in Fig. 4, which compares the best discharging patterns (potential versus charge recovered, normalised to mA h g^{-1}) at the three anodic limits (–0.60 V, –0.40 V, –0.20 V). In addition, Fig. 4 also shows that the ratio between charge extracted to –0.80 V and that integrated to –0.60 V (for uniformity in the three runs)

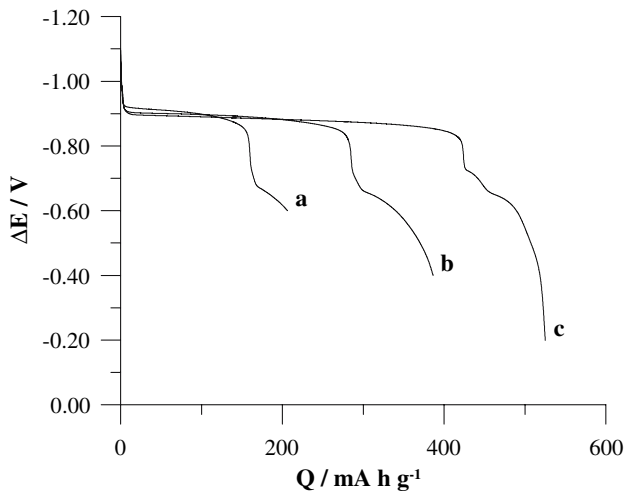

Fig. 4 Discharging patterns of the Fe sample for increasing anodic limits of the discharge: a = –0.60 V; b = –0.40 V; c = –0.20 V; ΔE (versus HgIHgO) in function of the charge passed, as mA h g^{-1}

increases from 0.76 to 0.82 and 0.88 with the respective discharge limits. In other words the charge bound to the Fe → Fe^{II} reaction increases at the expense of that extracted in the subsequent stage.

3.1.2 Steady-state i versus E experiment

Some elucidation of this activation process comes from the current-potential behaviour of the system, as shown in Fig. 5.

The curve formed by the full dots explains the behaviour of the Fe sample when, after complete discharge, it was left some tens of minutes at open circuit and then charged potentiostatically in steps, shifting the potential in the cathodic direction at any time. The curve given by the empty dots was recorded immediately, in the same way, after the first procedure - that is, with the electrode already charged. The cathodic current was smaller than before for most of the potential range, since the current in the first run was mainly due to Fe^{II} → Fe reduction, absent in the second run. However, at potentials negative to ≈–1.3 V, the two curves intersect, when the current (empty dots) exceeded that shown by full dots. The full squares curve was obtained when the charged electrode had been left for much longer under cathodic polarisation, then left at open circuit for a short time, and finally polarised again by steps in the cathodic direction. It is thus seen that, except for the initial part, the cathodic current definitely exceeds that attained in both the preceding runs.

In other words, prolonged cathodic polarization appears to activate hydrogen evolution, and this fits some findings, whereby long-lasting hydrogen discharge on Fe in alkaline

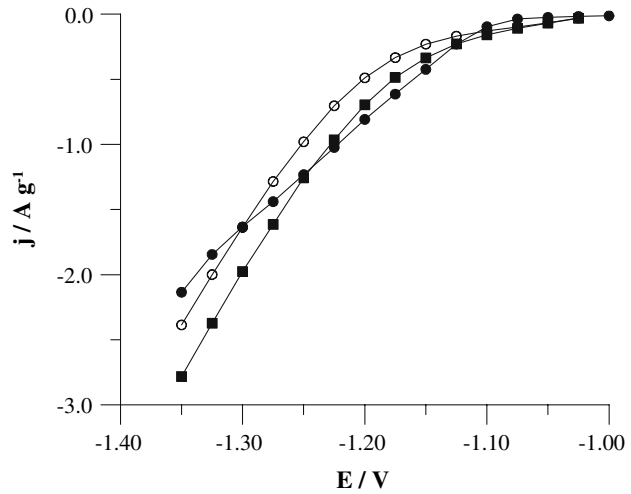

Fig. 5 Steady state potentiodynamic current versus potential characteristics of the Fe sample. Full dots curve was obtained from the fully discharged electrode; empty dots curve was recorded immediately after the previous one; full square curve resulting after having submitted the sample to hydrogen evolution for several hours

media induces significant variations into h.e.r. kinetics—for instance, favouring the entry of hydrogen into the metal [17].

3.1.3 *Coulombic efficiency*

The runs of Fig. 3 were performed by supplying, during charging, a current amount largely exceeding theoretical capacity, since the experiment aimed at activating charge storage in the sample as fully as possible. Therefore, when discharging maximum storage capacity seemed to have been achieved for each potential limit adopted, some runs were designed to determine coulombic efficiency between charging/discharging. These runs were performed by supplying only the current amount corresponding to the attained capacity (of the $Fe \rightleftharpoons Fe^{II}$ process) and using the same galvanostatic current intensity (–/+ 40 mA) in both charging and discharging.

Figure 6 shows the charging/discharging patterns obtained in succession with the four anodic limits (–0.60 V, –0.40 V, –0.20 V, –0.75 V), in which the charge supplied was recovered in two steps for all except the last (–0.75 V). Table 1 lists the coulombic yield related both to $Fe \rightleftharpoons Fe^{II}$ and overall discharge: the last column of the table shows the percentage of the theoretical capacity of the former. It is thus seen that for runs 18, 37 and 66 (with anodic limits of –0.60 V, –0.40 V and –0.20 V, respectively) overall yield was almost quantitative but, when the cathodic charge supplied was related only to that recovered at –0.80 V (by the useful $Fe \rightarrow Fe^{II}$ reaction), coulombic efficiency was in the range 67–75% or below. For run 106, with –0.75 V as anodic limit, coulombic efficiency was extremely high (95%), although this value may be considered totally exceptional, since it was obtained after the sample had been activated by prolonged reduction overnight. Repeated charging/discharging does show both decline in capacity and loss of coulombic efficiency. The data of Table 1 indicates that the maximum charge capacity engaged in the runs was $\leq 27\%$ of theoretical sample capacity.

3.2 Composite Fe/Oxide electrodes

3.2.1 *40/60 Fe/Oxide composites*

The previous section shows that only a fraction (<30%) of nominal electrode capacity can actually be exploited after a ''reasonable'' cathodic charge transfer. This result is in line with the literature, in which this problem is generally faced by increasing the porosity (i.e., the surface) of the Fe electrode, for instance, by mixing Fe with a chemical suitable for leaching from the manufactured electrode [10]. Instead, one recent approach consists of using Fe/C composites, in which the nano-carbon additive is expected to improve electrical conductivity at any discharge stage [12, 13].

This section deals with results on Fe/metal oxide composites, aimed at studying the effect of the particular ''dilution'' of Fe with a nominally inactive material. Figure 7 illustrates the evolution of charge capacity with number of cycles for three samples, consisting of Fe 40% in weight and 60% of various other metal oxides: their characteristics are listed in Table 2. The experiment was carried out by the same procedure as that of Fig. 3, by decreasing only discharge current intensity (from 40 to 20 mA) owing to the lower capacity of the samples; the anodic limit was either –0.40 V or –0.60 V for Fe/TiO_2.

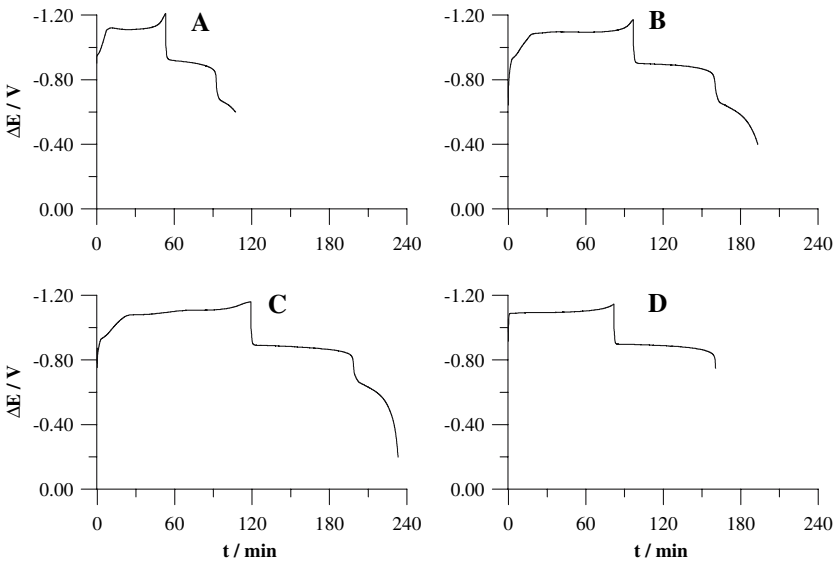

Fig. 6 Charging/discharging (–/+40 mA) potential vs time curves of Fe sample for different anodic limits of the discharge: **A** = –0.60 V; **B** = –0.40 V; **C** = –0.20 V; **D** = –0.75 V

Table 1 Coulombic yield of charging/discharging Fe powder electrode

Run no	Anodic limit (V)	Charge supplied (mA h)	Charge recovered		Charge recovered		Practical/Theoretical storage (%)
			At –0.800 V (mA h)	At >–0.800 V (mA h)	At –0.800 V (%)	Overall (%)	
18	–0.60	36.66	26.38	10.11	72.0	99.5	13.3
37	–0.40	66.66	42.50	22.60	63.8	97.7	21.4
66	–0.20	81.94	53.52	23.58	65.3	94.1	26.9
106	–0.75	56.11		53.33		95.5	26.8

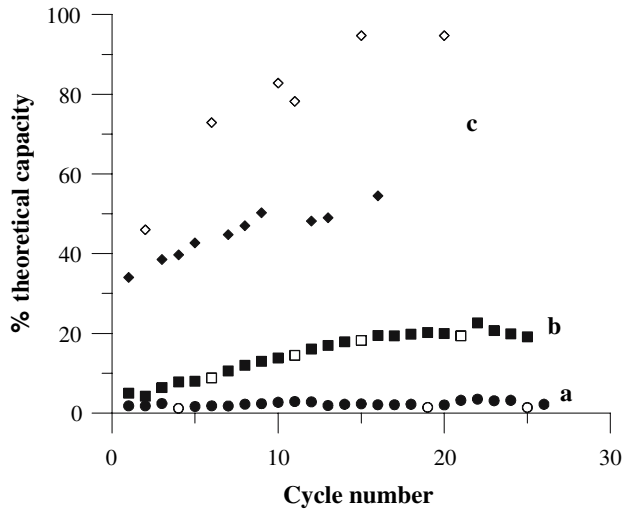

Fig. 7 Evolution of charge capacity of 40/60 (by weight) Fe/Oxide composite electrodes with number of charging/discharging cycles. Curves: a = Fe/Al_2O_3; b = Fe/ZrO_2; c = Fe/TiO_2. The meaning of the full and empty symbols were the same as in Fig. 3

Table 2 Characteristics of the Fe/oxide mixed powder electrodes

Composition/ weight (%)	Dimensions[(a)] (cm^2)	Fe content (g)	Theoretical capacity (mA h)
40/60 Fe/Al_2O_3	1.20 × 2.00	0.065	62.4
40/60 Fe/ZrO_2	1.15 × 2.00	0.056	53.8
40/60 Fe/TiO_2	1.20 × 2.00	0.051	49.0
70/30 Fe/ZrO_2	0.85 × 2.00	0.149	143.0
70/30 Fe/ZnO	0.80 × 2.00	0.078	75.0[(b)]
70/30 Fe/TiO_2	0.65 × 2.00	0.157	151.2

(a) Electrode thickness ≤ 0.10 cm

(b) Only referred to Fe content

Curve a of Fig. 7 shows that Fe mixed with Al_2O_3 practically loses all charge storage ability, as if the fine Al_2O_3 powder were acting as an inhibitor of Fe corrosion (i.e., Fe oxidation). The situation improves for Fe/ZrO_2 (curve b), but charge storage never exceeds ≈20% of the theoretical sample capacity.

Conversely, curve c shows that activation rate and attained capacity both improved remarkably with the Fe/TiO_2 composite, although the anodic limit of discharge settled at –0.60 V. The charge extracted from the sample after fast charging in a few cycles did reach ≈50% of the theoretical value, whereas that recovered after 15 h of slow rate charging more or less fitted nominal capacity. The pattern of this last run is shown in Fig. 8: discharge occurs in a single oxidation stage.

3.2.2 70/30 Fe/Oxide composites

This section deals with three 70/30 Fe/oxide samples, with Fe as the richer component and ZrO_2, ZnO and TiO_2 as the respective oxide partners. Sample characteristics are listed in Table 2. The behaviour of the Fe/ZrO_2 composite did not substantially differ from that of the 40/60 analogue: the increased Fe in the sample did not improve the percentage of its exploitable capacity.

Instead, the Fe/ZnO electrode is worth discussing, since ZnO, unlike the other oxides used here, can undergo reversible oxidation/reduction in alkaline media. The behaviour of the sample is clear in the discharge patterns of Fig. 9, which shows various stages of electrode life:

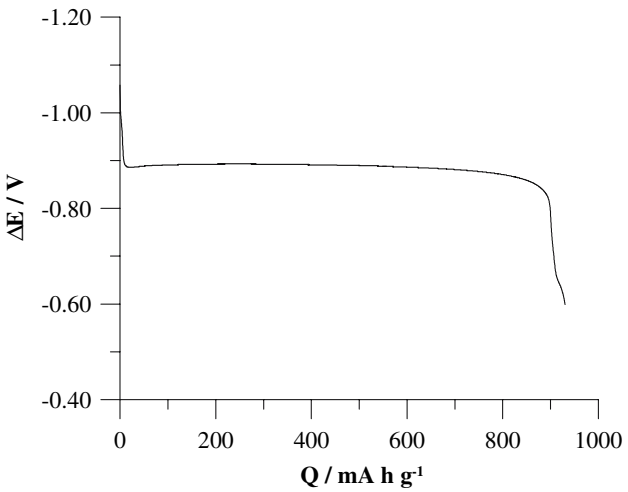

Fig. 8 Discharging pattern of the 40/60 Fe/TiO_2 sample after electrode activation and prolonged charging. The charge in the abscissa (normalised to the Fe content) almost fit the theoretical prevision

discharges were usually carried out at 30 mA and charging at –200 mA for ≤ 1 h. The first discharge (curve a) is dominated by Zn → Zn^{II}, which is negative to Fe → Fe^{II}. However, as soon as some Fe starts to be reversibly driven, the reduction of ZnO is increasingly hindered, as the galvanostatic charging current is mainly pinned at the more positive potential of both Fe^{II} → Fe reduction and hydrogen evolving on Fe: thus, Fe oxidation prevails even after 5 cycles (curve b). Within 5 more cycles Fe activation reaches 47% of theoretical capacity (curve c) and with 10 more cycles charge storage is at 64% of full capacity (curve d). After this charge capacity declines and, after 10 further cycles, it is reduced to less than 50% of the previous maximum (curve e). However, in this last case a large amount of charge is left in the sample, which could be extracted but at a much slower oxidation rate than before (i.e., <10 mA).

The 70/30 Fe/TiO_2 composite confirmed the good performance of the similar 40/60 sample: activation rate was slower than in that shown in Fig. 7 but, after fast charging, ≈50% of theoretical capacity could be exploited with 40 mA applied and ≈60% was obtained after prolonged slow charging. The composite did not show any decline in capacity in over 50 cycles and tolerated high discharging rates very well as Fig. 10 shows. The discharging patterns were obtained at 40.60, 91.35 and 122.25 mA: in each case a well-defined plateau took shape and the engaged fraction of theoretical capacity ranged from 51 to 33 and 19%. Instead, coulombic yield was lower than that measured in the pure Fe sample. This is inferred from the insert of Fig. 10, where the loss of balance between charging/discharging (at –/+ 40 mA) gives a coulombic yield of ≈55%.

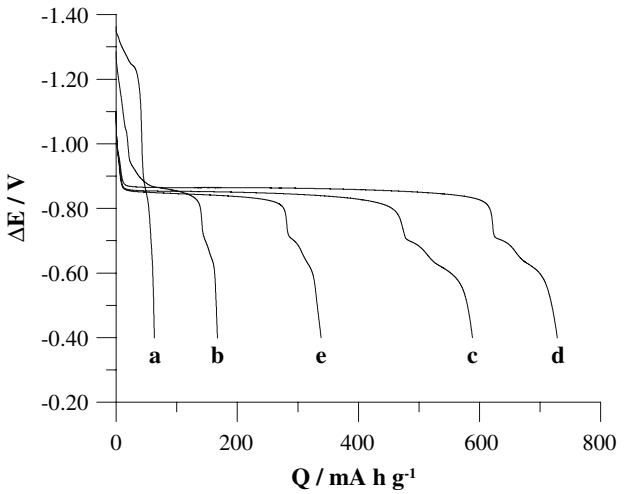

Fig. 9 Discharging patterns of the 70/30 Fe/ZnO composite electrode at different stages of its cycle life: the charge in abscissa was normalized to the Fe content only. The curves were recorded in the order: a = after one cycle; b = after 5 cycles; c = after 10 cycles; d = after 20 cycles; e = after 30 cycles

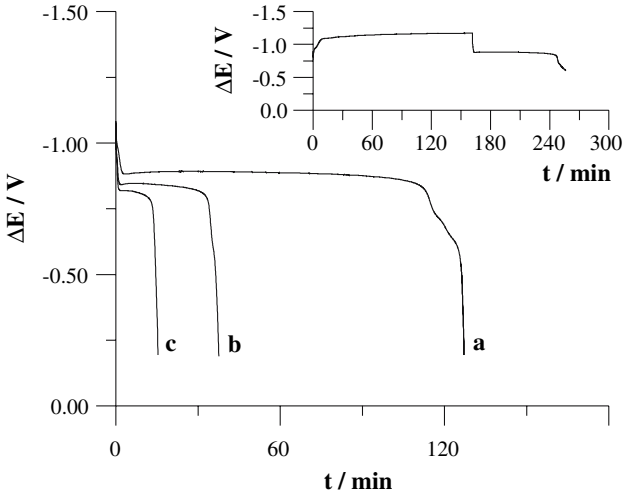

Fig. 10 Discharging patterns of the activated 70/30 Fe/TiO_2 composite electrode at different discharging rates: a = 40.60 mA; b = 91.35 mA; c = 122.25 mA. The insert account for the full charging/discharging (–/+40 mA) potential versus time plot of the sample

Although the charge supplied here was ≈70% of theoretical capacity the coulombic yield of the discharge did not exceed 60%, even when current amounts below 50% of theoretical capacity were supplied.

3.3 Composite Fe/IMC electrodes

3.3.1 Fe/$LaNi_5$ composites

This section reports results obtained by using Fe mixed with an intermetallic compound able to absorb hydrogen. The results of tests on Fe/$LaNi_5$ electrodes are shown in Fig. 11, which illustrates the discharging patterns of three different compositions (characteristics are listed in Table 3). Charging/discharging was performed at a reduction current of –200 mA × 50 min, followed by oxidation at a rate of 40 mA.

Curve a of Fig. 11 shows the performance of a pure $LaNi_5$ electrode, achieved after a dozen activation cycles: the charge capacity outlined by the plot, ≈ 230 mA h g^{-1}, which is the practical limit of the $LaNi_5$ specimen in these conditions, corresponds to ≈60% of the theoretical capacity of the corresponding $LaNi_5H_6$ hydride. Longer cycling resulted in a decline in capacity, as expected for a pure $LaNi_5$ intermetallic compound [18].

Curve b, referring to a 50/50 (by weight) Fe/$LaNi_5$ composite, shows a shape similar to that of curve a, Fe engagement in discharge being indicated only by the inflection occurring at –0.66 V versus Hg|HgO. Charge capacity is still dominated by the hydride: in fact, assuming that $LaNi_5$ is driven at the efficiency of curve a, at least 70% of the charge was bound to hydrogen extraction and

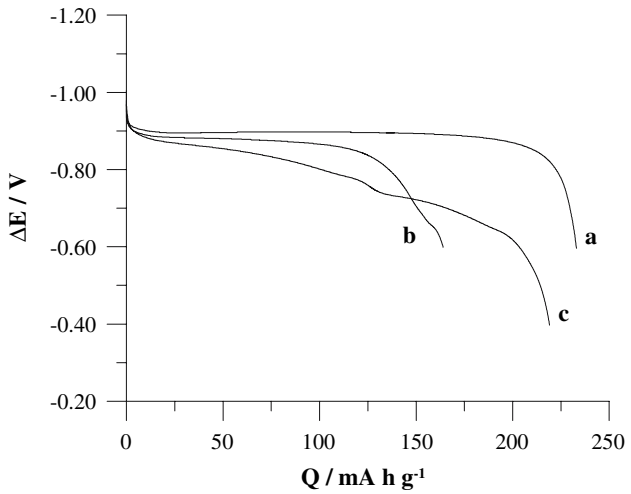

Fig. 11 Discharging patterns of respectively: a = pure $LaNi_5$ electrode; b = 50/50 Fe/$LaNi_5$ composite; c = 70/30 Fe/$LaNi_5$ composite electrode

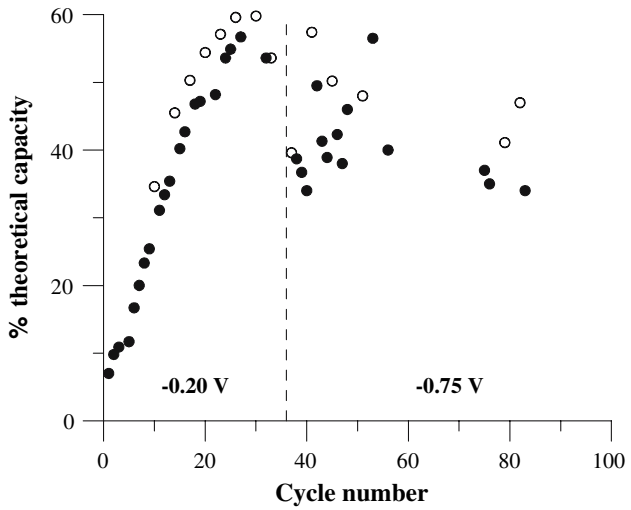

Fig. 12 Evolution of charge capacity of the 70/30 Fe/TiNi composite electrodes with number of charging/discharging cycles. The charge is given as percent of the theoretical (Fe + TiNiH) capacity. Other conditions were the same as in Fig. 3

Table 3 Characteristics of the Fe/IMC mixed powder electrodes

Composition/ weight (%)	Dimensions(*) (cm^2)	Fe content (g)	Theoretical capacity	
			IMC (mA h)	Fe (mA h)
100 $LaNi_5$	0.75 × 2.00	(–)	79.4	(–)
50/50 Fe/$LaNi_5$	0.65 × 2.00	0.115	42.9	110.4
70/30 Fe/$LaNi_5$	0.65 × 2.00	0.155	24.8	148.8
70/30 Fe/TiNi	0.60 × 2.00	0.126	14.0	121.0

(*) Electrode thickness ≤ 0.10 cm

the contribution of Fe was less than 10% of its nominal capacity.

Curve c shows the discharge of the 70/30 Fe/$LaNi_5$ composite. The pattern was recorded after more than 30 activation cycles and the anodic limit was also increased from –0.60 V to –0.40 V. The shape of the curve indicates the occurrence of two successive processes, i.e., hydrogen extraction and Fe oxidation: the former, again based on the experimental capacity of the pure $LaNi_5$ sample, still accounts for at least 50% of the whole charge storage, whereas Fe engagement was far less than its nominal capacity.

In conclusion, the electrochemical characteristics of the IMC appear here to dominate the electrode behaviour of the composites by totally or partially inhibiting Fe redox reactions.

3.3.2 Fe/TiNi composites

Figure 12 shows charge storage in a 70/30 Fe/TiNi sample (see Table 3) activated, with the number of charging/discharging cycles. As in Figs. 3 and 7, full dots refer to discharge at 40 mA after fast charging, and empty dots data obtained after 15 h of low current reduction (–40 mA); until run 33 the potential limit of discharges was –0.20 V and thereafter –0.75 V. The charge capacity measured at each cycle is given as a percentage of the theoretical capacity of the mixture, i.e., ≈750 mA h g^{-1}, assuming that TiNi is stoichiometrically converted into TiNiH hydride. Therefore, with –0.20 V as anodic limit, activation after fast charging was ≈40%, which increased to ≈50% after prolonged reduction, both figures being better that those attained with the pure Fe sample. With –0.75 V as anodic limit, capacity measured after fast charging declined smoothly with number of cycles, but in any case recovered after prolonged reduction. In practice the behaviour of pure Fe was reproduced.

Figure 13 shows some charging/discharging (potential versus time) patterns, all performed at the same rate (–/+ 40 mA) but with different charge periods. The coulombic efficiency between charge and discharge is seen to decrease with reduction of the composite from 87% to 76%, 66% and 60% (curves a, b, c, d), but the percentage of nominal capacity thus engaged increased from 26% to 31%, 37% and 42% respectively. In other words, coulombic efficiency is not only far better than for Fe/TiO_2 composites, but also compares favourably with the results of pure Fe (Table 1), with the exclusion of run 106. However, the last Fe datum was rather sporadic and in any case represented only about a quarter of the theoretical capacity.

The formation of the $TiNiH_x$ hydride could not be confirmed by X-ray analysis. In fact, according to the

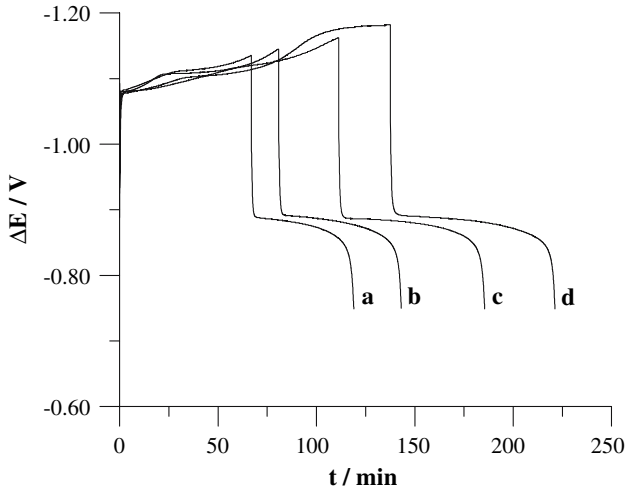

Fig. 13 Charging/discharging (–/+40 mA) patterns of 70/30 Fe/TiNi sample for reduction times increasing in the order a, b, c and d

diffraction pattern of Fig. 14A, the original TiNi powder supplied by Goodfellow has a very low crystallinity grade, so that only weak peaks due to Ti_2Ni traces were identified. Milling with Fe further increased the amorphous nature of the IMC, and the diffraction pattern of the mixture (Fig. 14B) only accounts for the presence of Fe.

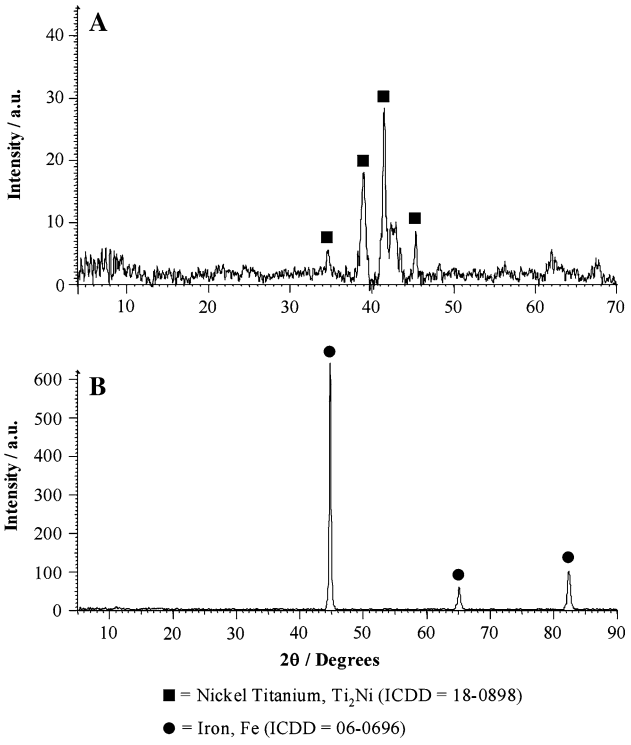

Fig. 14 X-ray diffraction patterns of: (**A**) TiNi as received from Goodfellow; (**B**) 70/30 Fe/TiNi powder mixture obtained from milling

4 Discussion

The charging/discharging runs, performed in order to increase the anodic limit of discharge, unambiguously demonstrate that deep oxidation of the Fe electrode has a positive effect on both charge capacity activation and the maintenance of that capacity. In fact, when the anodic limit was restricted to include only the Fe $\rightarrow$ Fe^{II} plateau, charge capacity generally showed a decline, which could be offset by again deepening discharge or by prolonging charging duration. In both cases, the coulombic efficiency of the useful Fe $\rightarrow$ Fe^{II} reaction (which can be very high only in particular circumstances; Fig. 6d) decreases to 65–75%. We explain this behaviour by the fact that deep oxidation of the electrode surface inhibits h.e.r. on it for some time, so that reduction of Fe oxides/hydroxides takes place very efficiently. This view stems from the results of Fig. 5 which show how the reduced Fe electrode becomes more and more electrocatalytic toward h.e.r.

The second point re-examined here concerns the discharge occurring positive to the Fe $\rightarrow$ Fe^{II} reaction. As mentioned in the Introduction, this discharge is generally ascribed to oxidative conversion of Fe^{II} into Fe^{III}: the lack of well-correlated stoichiometry between the two stages may thus be due to the slower kinetics of the latter with respect to the former. Conversely, this view is questioned by the data: as the charge extracted at the Fe $\rightarrow$ Fe^{II} plateau gradually approaches the theoretical capacity of the electrode, the charge involved in the latter oxidation diminishes. The limiting case was achieved with the 40/60 Fe/TiO_2 composite on which, after a charge amounting to about the theoretical capacity (Fig. 8) had been extracted at the Fe $\rightarrow$ Fe^{II} plateau, no further oxidation was detected.

It therefore appears that the formation of Fe^{III} species (FeOOH, Fe_2O_3, Fe_3O_4), without requiring the Fe^{II} intermediate, occurs mainly straightaway by, for instance:

$$3\,Fe + 8\,OH^- \rightleftharpoons Fe_3O_4 + 4\,H_2O + 8\,e^-$$

A pathway of this type, already suggested for Fe oxidation in 1 M LiOH at high temperature and pressure [19], would occur at the expense of the Fe $\rightarrow$ Fe^{II} reaction, when the outer $Fe(OH)_2$ layer precipitated on the electrode causes an excessive increase in electrical resistance which, in galvanostatic conditions, shifts the electrode potential to positive. This view is also supported by the well-known fact that a deeply discharged electrode can quickly regain the potential of the Fe $\rightarrow$ Fe^{II} redox reaction at open circuit, so that the residual charge still present in the electrode is mainly extracted along the plateau of that reaction, when a slower oxidation rate than before is applied.

The above shows that the charge capacity actually exploitable from the Fe sample appears to be limited, either by low charging efficiency due to concurrent h.e.r., or by hindrance of electrical resistance during discharge. To tackle these two problems, a route adopted since Edison's times [1] consists of mixing Fe powder with powders of other metals such as Cd, Cu, Pb, etc. [2, 3]. These metals, which increase both the hydrogen overpotential and the conductivity of the system, do not require comment. Instead, we discuss here the reason for the performance of Fe/Oxide and Fe/IMC composite electrodes.

In the Fe/Oxide samples, dilution of the active material (Fe) with a resistive and nominally inactive compound (all the oxides except ZnO) greatly affected electrode performance according to the nature of the oxide.

Thus, the inhibiting effect on the charge capacity of Fe, tested for the Fe/Al_2O_3 and Fe/ZrO_2 composites is quite easy to explain. When these oxides strongly interact with Fe in the mixture the surface of the Fe particles is expected to be partially shielded from the electrolyte, with consequent hindrance of the charging/discharging process. Instead, the Fe/ZnO composite showed fast activation to more than 60% of Fe theoretical capacity, then declining rather sharply. This behaviour is explained as follows. After the initial engagement in the charging/discharging process ZnO undergoes dimensional changes and partial dissolution as $Zn(OH)_4^{2-}$ in the strongly alkaline medium so that the surface of the Fe particles contacting the electrolyte greatly increases, not only with respect to its initial state, but also to that of the particle situation in a pure Fe pressed powder electrode. Maximum Fe capacity was reached during these runs. The later drop in charge capacity was more apparent than real, since a large amount of charge could be extracted, but at a discharging current much smaller than before. The low tolerance to the current was probably due to mixed Zn and Fe hydroxides being deposited on the electrode.

Although the characteristics of electrochemical inactivity and insolubility (experimentally tested for our specimens) of TiO_2 are much closer to those of ZrO_2 and Al_2O_3 than to those of ZnO, the Fe/TiO_2 composites showed totally unpredicted behaviour.

Electrode performance not only approached the fast activation and capacity level of the Fe/ZnO sample but, unlike it, the charge capacity attained by Fe/TiO_2 was steadily maintained, with very good tolerance of high discharging rates (Fig. 10). In other words, the Fe/TiO_2 electrodes performed better than the pure Fe analogues, except for coulombic yield, which was generally <60%.

We have no explanation for this result, but the presence of Li^+ ion in the electrolyte may be invoked, as happened for Fe_3O_4 reduction (see Fig. 2). Li^+ is known to intercalate easily into atanase and rutile from aprotic media [20, 21], and this process may transitorily occur in strongly alkaline electrolytes, as reported for other oxides [22]. In a recent study Li insertion into TiO2 in aqueous solution is reported [23], but in this case the TiO_2 was a nanostructured or mesoporous film formed by a surfactant template method. Our samples are different but, if the intercalation process still works, the intercalated compound may locally constitute micro-galvanic chains with the resistive Fe oxides, contributing to their reduction. In addition, the continuous formation/decomposition of the Li^+/rutile intercalation system may contribute to both dimensional changes and local high electrolyte concentration, sustaining high charging/discharging rates. Another support for this hypothesis is given precisely by the low coulombic efficiency between charging and discharging: it seems unlikely that this is due to increased hydrogen evolution on the resistive TiO_2 particles.

As a last observation on the different capacity showed by Fe/TiO_2 composite electrodes between fast and slow charging programs, as shown in Fig 7 (curve c, full and empty symbols). We have no explanation for this behaviour, but if Li^+ intercalation is the key process in the reduction mechanism of these electrodes an influence of concurrent hydrogen evolution may be invoked.

As regards the Fe/IMC composites the reason for studying their electrode behaviour is explained as follows. The major drawback of Fe, i.e. hydrogen evolution, is generally ameliorated by a suitable hydrogen inhibitor in either the electrode or the electrolyte: instead, the IMC present here in the electrode composition did not aim at inhibiting h.e.r., but at exploiting it. In other words, if the IMC is a good hydrogen absorber (for H_2 pressures of $\approx$ 1 atm), most of the hydrogen evolving on Fe during charging enters the IMC and the electric charge consumed is recovered in discharge. The resulting increase in coulombic efficiency with respect to pure Fe is not the major advantage expected from the Fe/IMC composite: in fact, if the IMC acts as an h.e.r. buffer, sealed operating conditions are allowed and the hydrogen pressure, in equilibrium with the IMC hydride, can significantly decrease the Fe corrosion rate (i.e., self-discharge). Last, but not least, the good electrical conductivity of the IMC mixed with Fe always favors full charge/discharge of the latter.

The above speculations are only hopeful, but they may be achieved in restricted compatibility conditions between Fe and IMC, clearly illustrated by the two composites chosen in this work. Results obtained with Fe/$LaNi_5$ electrodes thus demonstrate the total electrochemical incompatibility between the redox systems of the two components. This behaviour depends on the fact that $LaNi_5$ is not only an hydrogen absorber, but also a very good catalyst of the h.e.r., so that the hydriding process occurs positive to Fe^{II} reduction: the former reaction consequently

hinders the latter, and the redox potential of the forming $LaNi_5H_6$ particles is not sufficient to induce reduction of adjacent Fe oxide particles.

Conversely, the good preliminary results obtained with the Fe/TiNi composite, mainly due to the hydrogen overpotential, which is much higher on TiNi than on $LaNi_5$, demonstrate that good electrochemical compatibility can be achieved between Fe and hydrogen absorbing IMC. Therefore, proper choice of both the IMC (the number of hydride forming IMCs now available is very large) and IMC/Fe ratio may yield Fe electrodes of very interesting performance.

5 Conclusion

It has been shown that deep oxidation of the Fe electrode has a positive effect on the charging/discharging process and how a charge corresponding to the full theoretical capacity can be extracted at a single plateau process when a composite of iron with a suitable metal oxide is used as electrode. The first result is due to the inhibition of the hydrogen evolution reaction on the electrode surface and, the second to low electrical resistance during discharge. The results obtained with TiO_2 may be partially explained by the presence of Li^+ ions in the electrolyte and its intercalation into TiO_2.

Another route discussed in this work is the use of Fe/IMC composites as hydrogen absorbers. One of the most important properties that the IMC must show is a high hydrogen evolution overpotential, so that the hydriding process of the IMC occurs negative to Fe^{II} reduction. This is the case of TiNi for which the Fe/TiNi composite have shown good results.

This preliminary data suggest that Fe/IMC composite electrodes are promising if an appropriate IMC is found and the IMC/Fe ratio is optimised.

Acknowledgments The authors wish to thank U. Casellato (CNR ICIS, Padova) for X-ray analysis and for discussion of the results.

References

1. Falk SV, Salkind AJ (1969) Alkaline storage batteries. John Wiley & Sons, New York London Sidney Toronto, pp 16, 89, 305
2. Vijayamohanan K, Balasubramanian TS, Shukla AK (1991) J Power Sources 34:269
3. Chakkaravarthy C, Periasamy P, Yegannathan S, Vasu KI (1991) J Power Sources 35:21
4. Kordesh K (1981) In: O'M Bockris J, Conway BE, Yeager E, White RE (eds) Comprehensive treatise of electrochemistry, vol 3. Plenum Press, New York, pp 159
5. Öjefers L, Carlsson L (1977/1978) J Power Sources 2:287
6. Andersson B, Öjefers L (1979) In: Thompson J (ed) Power sources 7. Academic Press, London, pp 329–343
7. O'M Bockris J, Khan SVM (1993) Surface electrochemistry. Plenum Press, New York, pp 906
8. Ravikumar MK, Balasubramanian TS, Shukla AK (1995) J Power Sources 56:209
9. Periasamy P, Babu BR, Venkatakrishna Iyer S (1996) J. Power Sources 62:9; 63:79
10. Caldas CA, Lopes MC, Carlos IA (1998) J Power Sources 74:108
11. Souza CAC, Carlos IA, Lopes M, Finazzi GA, de Almeida MRH (2004) J Power Sources 132:288
12. Bui TH, Egashira M, Watanabe I, Okada S, Yamaki J, Yoon S, Mochida I (2005) J Power Sources 143:256
13. Bui TH, Watanabe T, Egashira M, Watanabe I, Okada S, Yamaki J (2006) J Power Sources 155:461
14. Edison TA (1907) U.S. Patent 876.445
15. Casellato U, Comisso N, Mengoli G (2006) Electrochim Acta 51:5669
16. Vassie PR, Tseung CC (1976) Electrochim Acta 21:299
17. Zakroczymski T, Szklarska-Smialowska Z (1985) J Electrochem Soc 132:2548
18. Kleperis J, Wojcik G, Czerwinski A, Skowronski J, Kopczyk M, Beltowsla-Brzezinka M (2001) J Solid State Electrochem 5:229
19. MacDonald DD, Owen D (1973) J Electrochem Soc 120:317
20. Kavan L, Fattakhova D, Krtil P (1993) J Electrochem Soc 146:1375
21. Fattakhova D, Kavan L, Krtil P (2001) J Solid State Electrochem 5:196
22. Li W, McKinnon WR, Dahn JR (1994) J Electrochem Soc 141:2310
23. Reiman KH, Brace KM, Gordon-Smith TJ, Nandhakumar I, Attard GS, Owen JR (2006) Electrochem Commun 8:517